Smart Agricultural Technology 8 (2024) 100449

Contents lists available at ScienceDirect

Smart Agricultural Technology

journal homepage: www.journals.elsevier.com/smart-agricultural-technology

Camera-based plant growth monitoring for automated plant cultivation with controlled environment agriculture

Tony Chen [a,b,*], Huiming Yin [c,b]

[a] Piedmont Hills High School, 1377 Piedmont Rd, San Jose, CA 95132, United States
[b] PVT Clean Energy LLC, 7 Industry St, Suite 5, Poughkeepsie, NY 12603, United States
[c] Department of Civil Engineering and Engineering Mechanics, Columbia University, 610 Seeley W. Mudd 500 West 120th Street, New York, 10027, United States

ARTICLE INFO

Keywords:
Camera
Plant growth monitoring
Algorithm
Controlled environment agriculture (CEA)
Smart greenhouse

ABSTRACT

Building integrated photovoltaic thermal (BIPVT) greenhouse technology exhibits great potential to enhance crop yielding, energy harvesting, and water management for highly efficient farming and enables controlled environment agriculture (CEA) for automated plant cultivation. The proposed smart greenhouse system uses BIPVT, geothermal, image-based sensing, and control technologies for high energy efficiency and high-fidelity plant growth control. A camera-based, computer-controlled system was demonstrated to successfully monitor single and multiple food plants' growth. The growth rate over the life-cycle of the plant was automatically recorded by cameras without human interference. A novel algorithm was developed to extract the plants from the background of the image and then to measure the length from the ground to the top of the longest plant with different shapes or profiles. The growth rate was automatically generated as fundamental data for farming management and control. Because the plant growth is slow and the errors caused by image noise can be comparable with the actual growth when the interval between images is not large enough, the noise of a camera is evaluated by comparing multiple images under the same exposure condition, which is used to provide the error range of the measurements. The plant growth monitoring system will be integrated into an ongoing greenhouse project for smart greenhouse operation.

1. Introduction

The summer of 2023 might be remembered as a heat-attacked season, as the temperature hits records in almost every corner of the world, crossing all the continents of the globe [1]. Climate change causes many consequences, but the impact on ecology and food output are among the top concerns. One of the main drivers of the food crisis is extreme weather events. Droughts, floods, and heat waves have damaged crops and livestock, leading to shortages of food supplies and price hikes as well. In this context, the issue of food deserts, where access to affordable, healthy food is limited, becomes even more pressing in disadvantaged communities [2].

The United Nations (UN) Food and Agriculture Organization (FAO) has warned that the number of people facing hunger could reach 928 million by the end of 2023, up from 828 million in 2021. The world's population is expected to reach 9.7 billion by 2050, and this will put a strain on our food production systems. In order to feed this growing population, we need to boost food production by 50% [3]. The situation is expected to get worse in the next decades as few actions have been taken to tackle the problems [4]. While the food crisis is a complex problem, among the measures that can be chosen, applying the latest technologies to boost the food supply is an immediate effort that will enhance food production.

Representing a shift in modern agriculture, on-site food production through Controlled Environment Agriculture (CEA) offers a potential solution with local fresh food supplies, which was enabled by the growth of crops in controlled greenhouse settings regardless of external weather conditions. CEA systems, which include hydroponic, aeroponic, and aquaponic setups, are designed to optimize plant growth conditions, thereby maximizing yield and resource efficiency [5]. This technology could mitigate the effects of extreme weather on food availability and offer a sustainable alternative for communities most at risk.

While CEA offers significant benefits in terms of yield and resource efficiency, the integration of advanced technologies presents challenges, including the complexity of data interpretation and the integration of technology, such as hyperspectral imaging, with existing agricul-

* Corresponding author at: Piedmont Hills High School, 1377 Piedmont Rd, San Jose, CA 95132, United States.
E-mail addresses: tonyyuchen2006@gmail.com (T. Chen), yin@civil.columbia.edu (H. Yin).

https://doi.org/10.1016/j.atech.2024.100449
Received 29 October 2023; Received in revised form 9 March 2024; Accepted 30 March 2024
Available online 5 April 2024

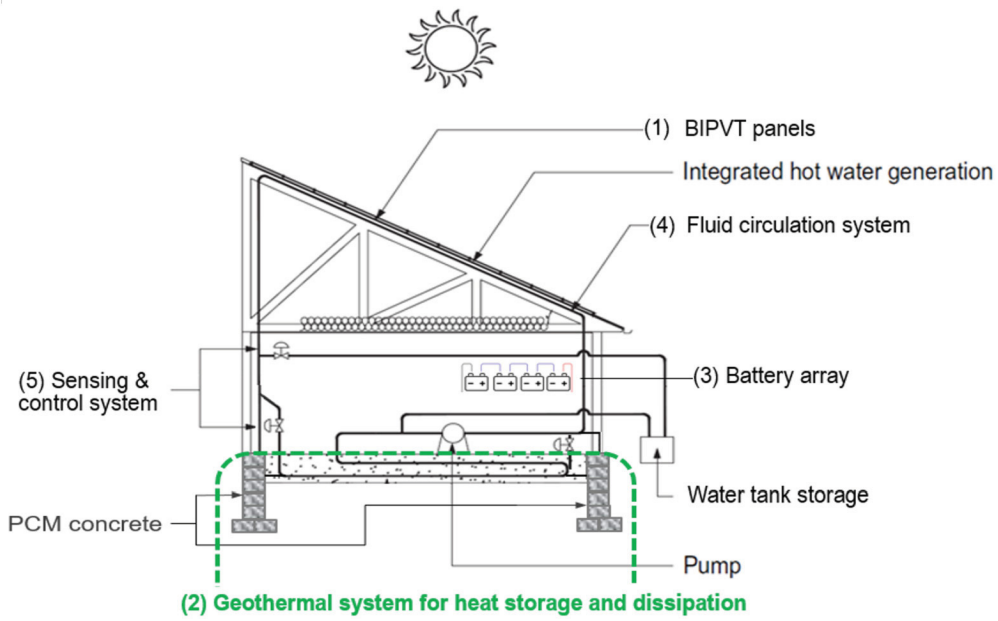

Fig. 1. Schematic illustration of a greenhouse system using BIPVT roofing panels and geothermal foundation [7].

tural systems [6]. These considerations highlight the need for ongoing research to optimize the application of these advanced technologies, such as imaging and analysis systems in CEA, to ensure their cost-effectiveness, scalability, and practicality in modern agriculture.

Recognizing these challenges, an innovative greenhouse model was developed that supports the integration of an imaging system for climate and light control. Fig. 1 shows a schematic design of an energy-efficient greenhouse that utilizes building-integrated photovoltaic thermal (BIPVT) panels, providing smart indoor environment control of light, temperature, and moisture for enhanced farm productivity and extended growing seasons. It can be scaled up depending on the farm's configuration, such as the arable land area, water availability, topographic form, as well as the demands of food and energy production. This CEA greenhouse design consists of five components: 1) advanced BIPVT panels for electricity and heat harvesting with a 25% coverage for a semi-transparent roof; 2) a geothermal system for seasonal heat storage and exchange in the geothermal heat well; 3) a battery array for electricity backup and storage; 4) a fluid circulation system with glycol for environment control and thermal management with a geothermal system; and 5) a sensing and control system for smart indoor environment monitoring and management for temperature, moisture, and light control [7].

The fifth component, the sensing and control system, will be the key to operating and managing the greenhouse for optimal system efficiency and plant growth. Estimating food plant growth health has traditionally relied on human inspection and experience for thousands of years. Decisions are made to irrigate, fertilize, get rid of pests and weeds, etc., based on the regular manual inspection, which can be destructive and highly depends on human factors, including the inspection frequency, inspector's knowledge, and sampling accuracy [8,9]. For large-scale farming, such traditional procedures may not be efficient. Automatic monitoring of food plant growth is a rapidly developing field and has attracted attention for deep exploration [10–12], because timely information can be extracted by computational analysis of images. Al-Karaki discussed data analysis methods that can be used to extract useful information from the data [13]. Zhang et al. discussed the different types of systems that have been developed and highlighted challenges such as inefficient microclimate control, high costs, and labor requirements [14].

Because plant growth is slow while image-taking is instantaneous, considering the noise of the camera and numerical errors in image processing, it is not trivial to extract useful information of plant growth from many images. High-fidelity image recognition is highly demanded in CEA and crucial for the precise control of applying water, fertilizers, and pesticides, which in turn minimizes waste and environmental impact. Error control mechanisms will ensure that the system responds effectively to any anomalies, thereby reducing the risk of crop failure and optimizing the yielding-cost ratio.

With the ultimate goal of designing and developing a solar and geothermal energy-based greenhouse for CEA farming, this paper particularly focuses on camera-based automatic plant growth monitoring, which will be integrated into the sensing and control system in future greenhouse construction. A high-accuracy camera-based automatic monitoring system was set up and demonstrated with the growth of wheatgrass. The system successfully monitors the plant growth rate and outputs the growth of the plant over a period of time on a daily basis. Inspired by the Breadth-First Search algorithm, this paper develops a novel technique to trace the plant's structure pixel by pixel, providing a more detailed and accurate representation of plant growth than conventional methods. As many existing systems rely on expensive and complex imaging technologies, the present approach utilizes standard cameras, allowing for accessibility and cost-effectiveness for widespread use in agriculture. Additionally, the method's non-destructive nature and adaptability to various plant species make it versatile across many applications. Furthermore, the algorithm and method can be generalized to an even wider variety of plants through physical data-based machine learning and plant growth modeling in future work.

2. System integration of the BIPVT greenhouse with geothermal energy

The proposed greenhouse in Fig. 1 utilizes building integrated photovoltaic-thermal (BIPVT) panels coupled with geothermal energy for the dual synergetic benefits: 1) improved energy harvesting and management toward zero-net-energy agriculture, 2) CEA with light, temperature, and moisture for improved plant production [7]. The advanced BIPVT panels with 75% transparent and 25% solar cell coverage will be installed on the south-facing roof of a solar greenhouse to generate PV electricity and collect heat; the electricity can be stored in a battery array for electricity backup and directly used for extended LED light for plant growth; a passive bi-directional geothermal heat exchange system will store heat in summer and release in winter by a

smart thermal management system and; the sensing and control system will monitor energy usage and distribution for smart operation. The holistic management of the heat, water, and air flows through the greenhouse will achieve high energy efficiency and economic benefits. Particularly, although the desirable environment for plant growth often mismatches with the daily weather, if we can store excess water and heat for future use, it is possible to achieve net-zero energy and net-zero water farming.

2.1. Equipment and hardware needed for the BIPVT greenhouse prototype

A small BIPVT greenhouse has been designed in coupling with the geothermal energy system for research purposes and will be constructed and demonstrated at Pleasant View Farm at Brewster, NY as a prototype for future large scale applications. The land plan is $24 \times 36 = 864$ sft. The materials and costs are much higher than the market price as they are ordered in a small amount by customized manufacturing, and the actual price by mass production can be much lower. The current price are listed as follows: the BIPVT roofing panels amount $\$17,320$ for glass-sun power modules, the greenhouse structure $\$34,420$ for polycarbonate panels and steel frame structures, the greenhouse installation fee $\$30,550$, the geothermal well drilling $\$16,420$. The total structure costs $\$98,710$. The monitoring and control units change with the research purpose for different case studies and are estimated $\$18,000$. Upon the successful demonstration of the system by case studies with actual plant growth, the research team will optimize the design with a goal of greenhouses $\$100,000$ for standardized green houses at 24×60 sft in the future, which can be scaled up and down to different sizes in approximately proportional costs.

2.2. Software for the operation of the smart greenhouse

Traditional control systems for the greenhouse are constructed to achieve the maximum crop production through the balanced environmental parameters for multiple control loops [15], which can be implemented by proportional, integral, and derivative (PID) controllers as follows:

$$u(t) = k_p e(t) + k_i \int_0^t e(t)dt + k_d \frac{de(t)}{dt} \tag{1}$$

where $u(t)$ is the control vector, $e(t)$ is the error of the signal, and k_p, k_i and k_d are the proportional, integral, and derivative constants, respectively [16]. When multiple controls are applied, such as heating, fogging, lighting, ventilation, and CO_2 flux, the above equation can be expanded into a matrix form. For different plants, different PID controls could be straightforwardly implemented in the present greenhouse. However, when the external environmental conditions change with the locations, weather, and seasons, the PID control may lead to unsatisfactory performance with large errors, high energy/water consumption, and failures due to the mismatch of the capacity and demand of the control system. Particularly, it is time-consuming to develop the control parameters for such a new greenhouse technology.

On the other hand, model predictive control (MPC) can be a better alternative to PID control to optimize the control based on the real-time sensing and modeling results, which significantly improves the robustness and efficiency of greenhouse management systems, particularly under frequent extreme weather due to climate change and global warming. MPC determines the optimal control sequence by minimizing the cost function, which can be constructed over a series of discrete time t_k $(k = 0, 1, \cdots, N)$ as an example [16]:

$$J(\mathbf{u}) = \frac{1}{2} \sum_{k=0}^{N-1} \left[x_i(t_k) Q_{ij} x_j(t_k) + u_m(t_k) R_{mn} u_n(t_k) \right] + x_i(t_N) P_{ij} x_j(t_N) \tag{2}$$

where $x_i(t_k)$ $(i = 1, 2, \cdots, N_s)$ are the total N_s state variables at time step t_k with $x_i(t_0)$ given by sensors, such as temperature, moisture, light, CO_2 level; $u_m(t_k)$ $(m = 1, 2, \cdots, N_c)$ are the total N_c state variables at time step t_k to be optimized in the range of $u_m^{min} \le u_m(t_k) \le u_m^{max}$; Q_{ij} and P_{ij} are semi-definite positive representing the cost of the state; R_{mn} is definite positive representing the cost of the control; the repeated subscripts $1 \le i, j \le N_s, 1 \le m, n \le N_c$ follow the Einstein summation notation [17]. A predictive model can predict the state variables as

$$\mathbf{x}(t_{k+1}) = f\left(\mathbf{x}(t_k), \mathbf{u}(t_k)\right) \tag{3}$$

Therefore, given the state variable at t_0, a quadratic cost function $J(\mathbf{u})$ can be constructed and solved by a quadratic optimization program [16]. Accurately sensing and monitoring the state variables is critical to greenhouse management and operation. Existing MPC platforms [18, 19] can be integrated into the present greenhouse to minimize the cost.

Although PID control systems are well established and can be installed into the BIPVT greenhouse in the initial phase, in the long term, an MPC control system is needed for the smart greenhouse as the environmental conditions can be optimized by balancing the cost-benefit ratio in a certain time window, to achieve the maximal benefit. The ultimate goal of the greenhouse is to maximize the yielding of plants to cover the costs with economical margins. Even though a high-performance environmental control system can create a growth environment accurately, it is critical to correlate the relationship between the environmental parameters and plant growth rate. Therefore, we can provide recipes of environmental control for different plants according to their growth pattern. Plant growth sensing and modeling not only provide inputs to control the environments but also enable machine learning to develop a predictive model with the actual plant growth data. A novel CMOS image-based sensing and modeling method has been developed and demonstrated in the next section, which will be integrated into the greenhouse for plant data collection.

The entity relation (ER) diagram of the sensing and control system is shown in Fig. 2 for the proposed smart greenhouse. Given a plant to grow in the greenhouse, we can formulate the recipe of desirable environment parameters and the expected growth each day in its life cycle. The environmental sensing will provide real-time monitoring of the greenhouse environmental parameters. When their difference from the recipe is larger than the threshold, it triggers the environmental control units to enforce the environmental change according to the recipe. The plant growth sensor will detect the growth rate against the recipe. If the difference is larger than the threshold, the recipe shall be updated through modeling and simulation. The operational data records provide the physics-based data for machine learning to optimize future plant growth recipes as well. The sensing and monitoring system will keep running with the greenhouse operation. The ER diagram provides the guideline for database construction and software development for system integration, which will directly monitor the environmental parameters through the hardware and control the work units by the commands from the software. This paper focuses on the plant growth sensing and monitoring.

2.3. Energy equilibrium in greenhouse operation

The energy flow in this greenhouse can be optimized by engineering the energy transfer and storage with the change of time and space with daily and annual energy equilibrium for electricity and heat, respectively, for a net-zero energy greenhouse technology. The solar panels harvest both photovoltaic (PV) and heat from solar irradiation. The electricity is stored in batteries for LED and greenhouse operation energy supplies, and the heat is stored in the earth for greenhouse heating.

A bi-directional geothermal coupling with BIPVT uses the thermal mass at a relatively stable temperature of the shallow earth only, so that it can be installed on-site of the greenhouse with low initial costs. A ground source heat pump system can be used for active temperature control. Based on the design of a bi-directional geothermal heat exchanger for BIPVT systems, the heat transfer between the greenhouse and the ground can be approximated as a harmonic variation on a daily

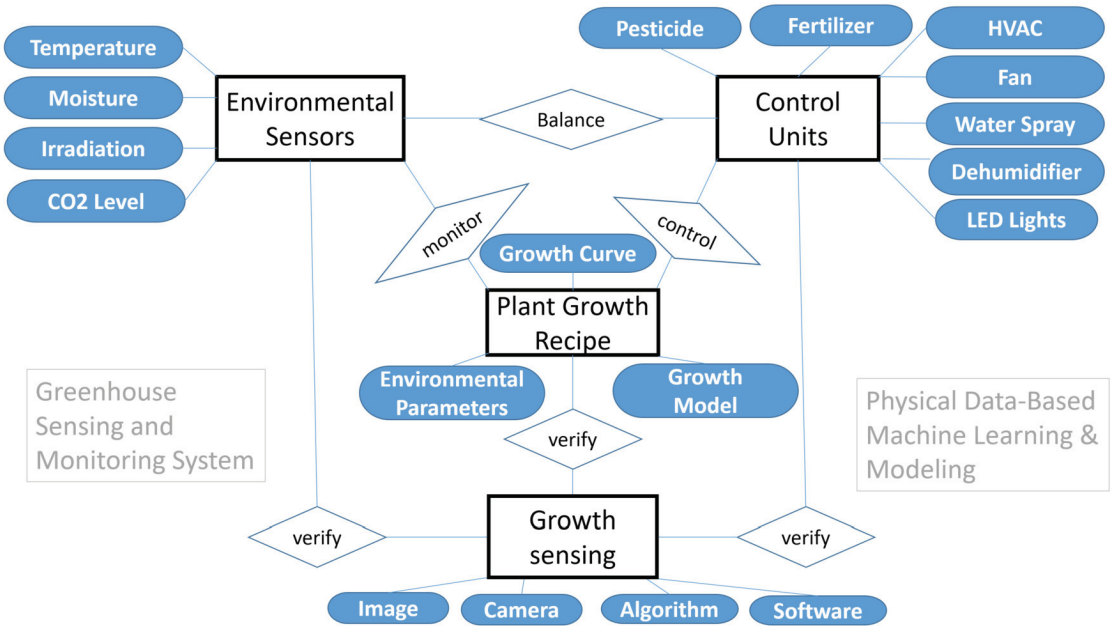

Fig. 2. The entity relation diagram of the sensing and control system for a smart greenhouse.

and annual basis in accordance with the angle of sunlight variations. The temperature profile of the ground will change with the distance to the geothermal heat exchanger. In summer, the thermal fluid takes the heat from the greenhouse to the ground, reducing the room temperature for indoor comfort. Seasonal heat storage can be achieved with the heat pipe at a certain depth higher than 20' so that the heat stored in summer may not be transferred to the ground surface before it is utilized in winter.

The energy equilibrium analysis of solar energy harvesting and system power consumption is an essential step that determines the capacity of energy storage and thermal fluid circulation systems. The energy level in the battery is traced throughout a prescribed period T, which is typically one day with a charge-discharge cycle, to aid the engineering design and to predict the system performance. The amount of energy charged into the battery is the difference between the harvested power and the consumed power. However, the daily equilibrium is not sufficient for areas with dynamic weather variation. Statistical analysis is required to determine the redundancy of the storage capacity. Because the average temperature change and heat needs strongly follow the season variation, heat storage and utilization will mainly be based on annual energy equilibrium.

Based on the power specifications of the control units, given a weather pattern and plant growth recipe, the energy consumption and harvesting can be calculated, and the zero-energy greenhouse can be designed through annual energy equilibrium.

3. Methodology of plant growth monitoring

CMOS image sensors replaced CCD (charge coupling devices) cameras and became the mainstream devices for different applications, largely because of their better performance and much lower prices [20]. The cost of cameras is no longer a barrier to its application to the agriculture industry. The most straightforward approach is to use RGB cameras to capture images of plants. These images can then be analyzed to detect changes in plant heights and provide information on growth rates. Hyperspectral cameras may figure out the wavelengths of the light that are reflected by the plants and can be used to identify different plant species [21]. Thermal cameras can detect the heat emission of plants to judge their health [22].

In this work, two regular color webcams were used to take images from different angles, and a computer-based Python program was written to control the cameras, extract the plant images from the background, measure the length of the plant, and generate the final growth rate table. The images in the procedure were saved for the purpose of demonstration, but in the real application, it is optional to save sample images up to the storage limits.

3.1. Calibration of the camera noise

When measuring objects at a small scale, camera noise may affect the accuracy of measurements. For example, if the end pixels of the plant are obstructed by camera noise, the algorithm may detect the plant to be longer or shorter than it physically is. Furthermore, large groups of noisy pixels that appear green may cause the program to incorrectly detect a plant present amidst the noise. Thus, measures were taken to minimize the camera noise surrounding the plant. The experiment was conducted in a brightly lit environment, and a Python program was created to evaluate the level of camera noise present and amplify it for visual clarity. Each pixel has a brightness value from 0 to 255, and any noise that causes a brightness difference of more than five levels, or a $\frac{5}{256} = 0.0195 \approx 2\%$ brightness difference from the original pixel is recorded and amplified. The threshold of five brightness levels was chosen to strike a balance between sensitivity to noise and the practical detection of meaningful discrepancies. This threshold is stringent enough to capture virtually all noise that could plausibly have an effect on the length calculation but avoids overestimating noise levels by disregarding minimal brightness variations that are extraordinarily unlikely to impact the overall accuracy of the image processing algorithm. The decision to set this specific threshold is further informed by preliminary tests, which indicated that a higher threshold (such as a 13 brightness level difference that would equate to approximately a 5% error tolerance) would result in a detection of virtually no noise, thus failing to adequately represent the small amounts of environmental noise present in the image data.

To test the amount of noise in the environment, Figs. 3(a) and (b) are two images taken with an identical setting, which leads to the difference shown in Fig. 3(c) due to the camera noise present in the testing environment. The white pixels indicate a difference of more than 2% between the two supposedly identical images, and black pixels indicate a lack of difference, suggesting that camera noise did not alter the pixel between when the two images were taken. Note that there is minimal camera noise affecting measurements, as the number of white pixels,

(a) Image 1 (b) Image 2 (c) Image Difference

Fig. 3. Evaluation of the camera noise: (a) and (b) two images taken with an identical setting, and (c) image difference with 2% as the threshold - non-negligible noise shown by white pixels and otherwise black pixels.

N_w is kept relatively low in comparison with the number of black pixels, N_b. The ratio of the white pixels to the overall pixels $\eta = \frac{N_w}{N_w+N_b}$ can be used to evaluate the noise impact on the image quality.

Because the camera noise has been produced by the total area of the image, it leads to an error range of the length at $\eta/2$. Fig. 3(c) provides $\eta = 0.00191$ for the image setting. Because the noise exhibits higher intensity along the boundary of the objects, the noise ratio η depends on the objects in the image or the background setting. Therefore, the calibration of noise shall be taken in the greenhouse periodically for consistency.

3.2. Determination of error due to pixel size

While the resolution of a camera is typically defined by the number of pixels in an image, we are more interested in the physical length of a pixel in the region of interest (ROI) of an image. For example, in Fig. 3, the height of the cup $H = 40$ mm covered by 65 pixels has been used as the reference, which corresponds to $L_p = 0.615$ mm per pixel in the ROI. Therefore, the accuracy of the image considering the effect of the camera noise is approximately at $\Delta = L_p * (1 + \eta/2) = 0.616$ mm, which can be used to determine the interval for image-taken in plant growth monitoring. The plant growth between two of a sequence of images shall be higher than Δ to capture sensible information. Depending on the plant growth pattern, we can tailor Δ with the camera's focus distance and resolution. In the following, we use wheatgrass as an example to demonstrate the algorithm for plant growth monitoring.

3.3. Algorithm for plant growth monitoring (2D)

Wheatgrass planted from seeds was chosen as the target plant in this study because it grows quickly, and therefore, the experiment can be reproduced within a week. The wheatgrass seeds were planted in small cups in Fig. 3, and once they grew out of the earth, the monitoring started. For the experiment, we established two distinct groups. The first group consisted of a single cup with one wheatgrass plant, while the second group involved a cup containing three wheatgrass plants. The cup plants were placed in a white background box, and cameras were set up to capture the plant growth.

A Python program was developed to control the cameras and command them to take pictures at predefined times and intervals, and here the images were collected once a day in the afternoon. The Python program also extracts the green pixels as the grass profile, and an algorithm based upon the Breadth-First Search (BFS) algorithm [23] was developed to accurately measure the length of the plants regardless of the growing direction, whose schematic is shown in Fig. 4.

The Breadth-First Search (BFS) is a fundamental algorithm in computer science used for traversing or searching tree or graph data structures. It starts at a selected node (in this case, a pixel at the base of the plant) and explores all of its neighboring nodes at the present depth

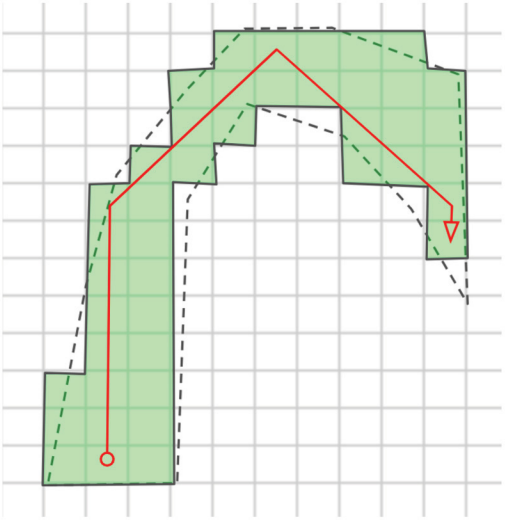

Fig. 4. Plant length measurement schematic. The background grid represents pixels, the dashed profile mimics a plant, green-filled pixels represent the image, and the red line reflects the length measurement procedure. Vertical and horizontal direction counts 1 unit per pixel, and diagonal counts 1.41 units per pixel.

before moving on to nodes at the next depth level. In our application, when an image is taken, green masks are applied to isolate the plant from its background. A starting point pixel is selected for each image, from which the BFS algorithm extends outward in all directions, including diagonally, traversing every connected green pixel until all green pixels are visited. The pixel farthest from the starting point is taken as the endpoint of the plant, and a path was traced back from the endpoint to the starting point to find the true length of the plant. Each time the path moves horizontally or vertically across a pixel, a length of one pixel was added to the measurement, and each time the path is traced diagonally across a pixel, a length of 1.41 pixels was added to the measurement. Since the red cup is a constant height of 4 centimeters, the height of the cup in pixels was used to convert the plant's length measurement into centimeters. Since there are two images, two measurements would be made, and the longer one of the two is used. Repeating the experiment over five days, the results were placed into a length-versus-time table as a fundamental reference for plant growth monitoring.

One camera can capture a 2D image and obtain a plant's silhouette in one orientation as a line constructed by many pixels. To improve the accuracy of measurements, the experiment instead utilized two cameras, each positioned at a 90-degree angle relative to the other. This was done for two reasons: 1) The use of two cameras positioned 90 degrees apart ensured that the plant's profile could be captured from multiple

(a) Raw Image (b) Red Mask (c) Green Mask (d) BFS Path

Fig. 5. A bent straw measurement showing the algorithm worked as expected.

(a) Raw Image (b) Red Mask (c) Green Mask (chosen plant) (d) BFS Path

Fig. 6. Three plants' measurements show the algorithm worked as expected.

angles, thereby eliminating blind spots and mitigating the risk of underestimating the plant's length due to bends or curves that might be hidden from a single camera's view. 2) The algorithm was designed to account for diagonal traversal with 1.41 pixels, as opposed to a simple one-pixel increment for horizontal or vertical movement. This nuanced approach to measurement allowed for a more accurate representation of the plant's true length, especially when the plant grew in a non-linear fashion. These deliberate steps were crucial in minimizing error and providing a more precise and reliable dataset for plant growth analysis.

3.4. Verification of the algorithm

To test the program, a green object of two sides at 65 and 82 mm, respectively, with a downward-pointing tip, was selected to check the system. Using the cup height as the reference, the program successfully measured the length of the object to a high degree of accuracy at 149 mm in Fig. 5.

Additionally, the cup with three plants was used to test the automatic program. The plants were grown and photographed in moderate humidity, 25 degrees Celcius temperature, and under high constant light. As shown in Fig. 6, after image taking, the program was able to identify the longest plant and only calculate the length of that plant. Of course, different schemes can also be predefined, for example, measure all 3 plants and calculate the average or median length, measure only the median plant, or only the shortest plant. In this study, the longest one was chosen, which has a length of 52 mm. The program successfully measured the length of the object to a high degree of accuracy at 54 mm in Fig. 6.

As verified by the two tests, the program functions properly in two difficult scenarios: 1) when confronted with sharp curves, the program finds its way through sharp angles; and 2) when multiple plants are detected, the program can distinguish the size of each and select the longer one to measure.

3.5. Expansion of the algorithm into 3D

For applications that require a particularly precise measurement or a 3D representation of the plant, a 3D version of the algorithm was developed. Because the path chosen by the algorithm is recorded for both cameras as image outputs whenever a measurement is made for each of the two cameras, it is possible to use these two image outputs in conjunction to create a 3D representation of the plant in a process known as voxel carving.

First, the two images are scaled (with their aspect ratio preserved) to the same height in pixels and are given a coordinate system, with one image having a horizontal X axis, the other having a horizontal Y axis, and both sharing the same vertical Z axis for height. Since they share the same Z axis, scaling both to the same height in pixels guarantees that both images are at the same scale in terms of pixels.

Then, one image is placed on the X-Z plane while the other is placed on the Y-Z plane, and both are extruded towards their remaining axis so that they intersect and pass through each other.

Voxels at the intersection point are occupied twice, meaning that both the extruded profiles contain them. These voxels, which are consistent with the information from both images, are kept, and the rest of the volume created by the extrusion—the voxels only occupied by one of the extruded profiles—is discarded. Through this process, a 3D object is constructed that, when viewed through either the X-Z or Y-Z profiles, will reflect the two 2D images taken of the real plant.

A demonstration of this method on Triple Plant B - Day 5 is shown below in Fig. 7.

Finally, after this approximate model of the plant has been created, we rerun the modified breadth-first search on the 3D model to find the shortest path from the bottom of the plant to the furthest tip, which will serve as the 3D algorithm's calculated height. In Fig. 7(c), the plant is measured at a length of 10.96 cm, showing a minor difference of 1.45% from the 2D measurement of 11.12 cm and 0.64% from the human measurement of 11.03 cm.

The Python program script was provided as the Supplementary Material of this paper.

4. Experimental demonstration of wheat grass growth monitoring

To demonstrate the program application in future greenhouse operations, we conduct an experiment with two groups of wheatgrass: group A with a single plant and group B with 3 plants. We monitored their growth with images taken continuously for 5 days. For demonstration, the images on days 1, 3, and 5 are provided as follows.

Fig. 8 shows the group A single plant situation on day 1. Camera-1 and camera-2 took images at different angles, and measurements using both algorithms were taken. The larger of the 2D algorithm's measure-

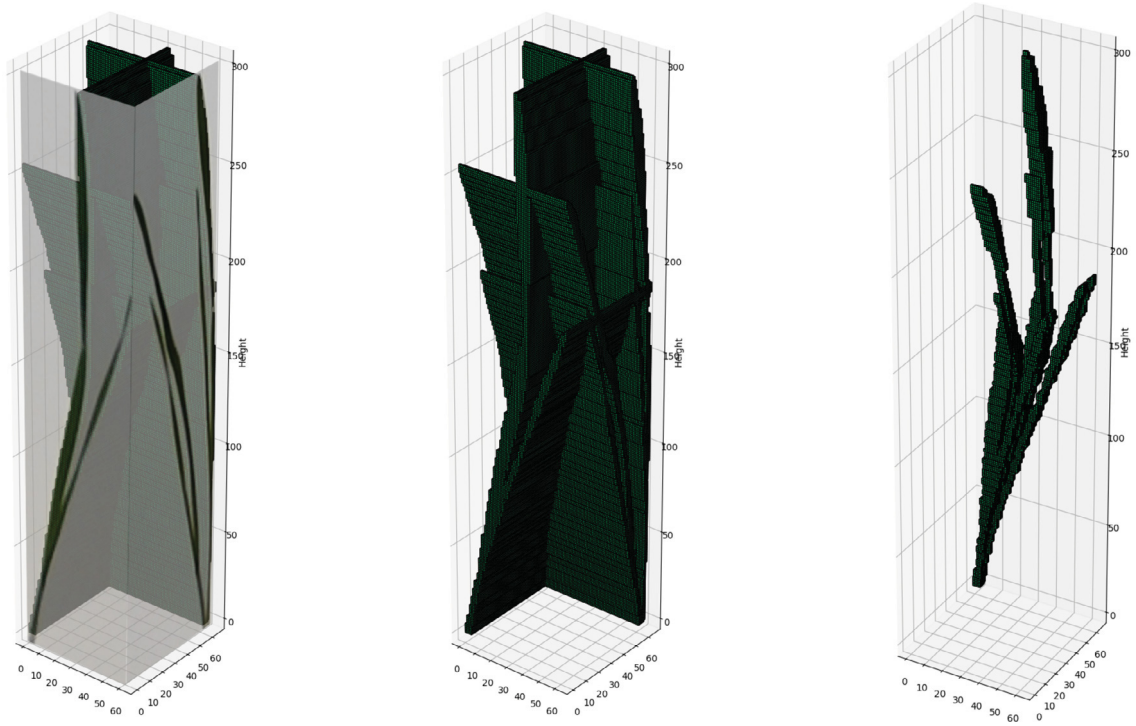

(a) Extrusion from Images (b) All Occupied Voxels (c) Voxels Occupied Twice

Fig. 7. Construction of 3D profile from two 2D images: (a) extrusions from the two 2D images, (b) the resulting object, and (c) the final object.

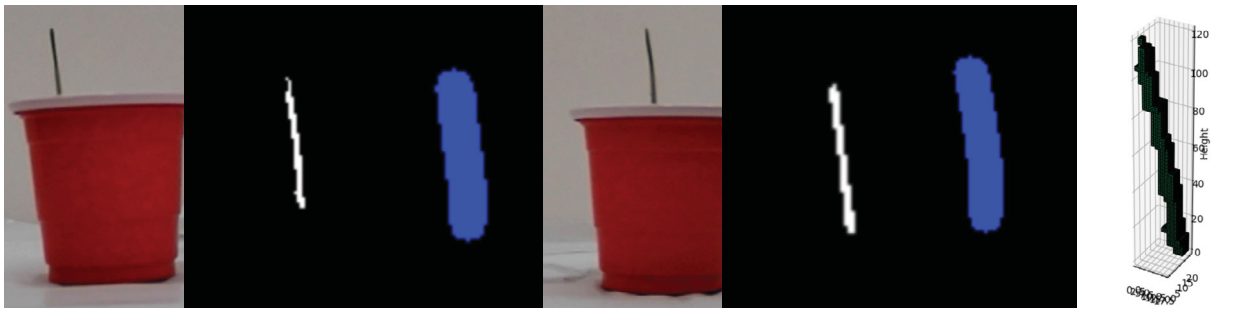

(a) C1 Raw Image (b) C1 Green Mask (c) C1 BFS Path (d) C2 Raw Image (e) C2 Green Mask (f) C2 BFS Path (g) 3D Representation

Fig. 8. Real images, plant information, and length measurements for group A single plant, day 1. C1 and C2 denote the cameras.

ments was recorded, and the single 3D measurement was recorded as the heights for Day 1.

Similarly, Figs. 9 and 10 show the progress on days 3 and 5, respectively. As seen in Figs. 10 (d) and (e), the program can detect the plant with multiple leaves and measure the longest stem as shown in (f) automatically.

Similarly, Figs. 11–13 show the situation of group B with three plants on days 1, 3, and 5, respectively. The program only extracted the image of the longest plant among the three and made the measurement. Again, the larger of the 2D algorithm's measurements were recorded, and the single 3D measurement was recorded as the plant heights.

On day 5, after all the information was collected and measurements were taken, the program outputs the growth curves for groups A and B, for each algorithm, as shown in Fig. 14. It was interesting to see both groups A and B shared similar growth rates and tended to become slower over time, and how the 2D and 3D algorithms produced estimates that were quite similar.

Table 1
Results for Single Plant A and Triple Plant B.

	Day	1	2	3	4	5
Single Plant A	3D Algorithm (cm)	1.75	4.55	6.99	10.01	10.41
	2D Algorithm (cm)	1.71	4.33	7.29	10.38	11.75
	Human Measurement (cm)	1.79	4.13	7.06	10.15	11.68
Triple Plant B	3D Algorithm (cm)	2.93	5.19	7.55	9.54	10.96
	2D Algorithm (cm)	2.83	5.16	7.79	9.80	11.12
	Human Measurement (cm)	2.82	5.48	7.60	9.28	11.03

The lengths of the plants were also measured by hand and compared with the image-based results in the following tables. It is important to note that "human measurement" is distinct from "real length" as it is unfeasible to measure a precise definitive length. The particular reasons will be explained below.

As displayed by the table above, while all three forms of measurement produce similar heights, each has its own sources of error.

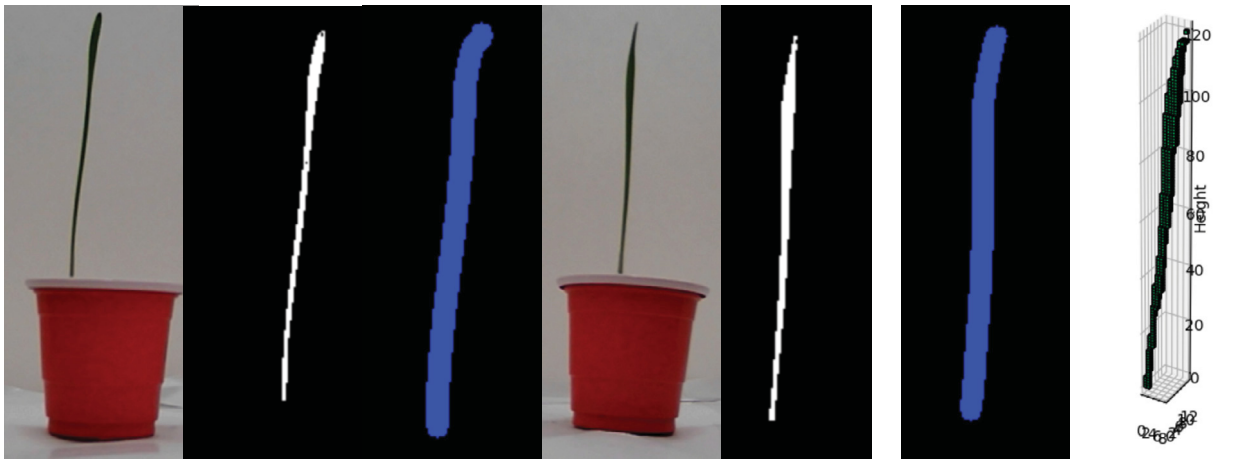

(a) C1 Raw Image (b) C1 Green Mask (c) C1 BFS Path (d) C2 Raw Image (e) C2 Green Mask (f) C2 BFS Path (g) 3D Representation

Fig. 9. Real images, plant information, and length measurements for group A single plant, day 3.

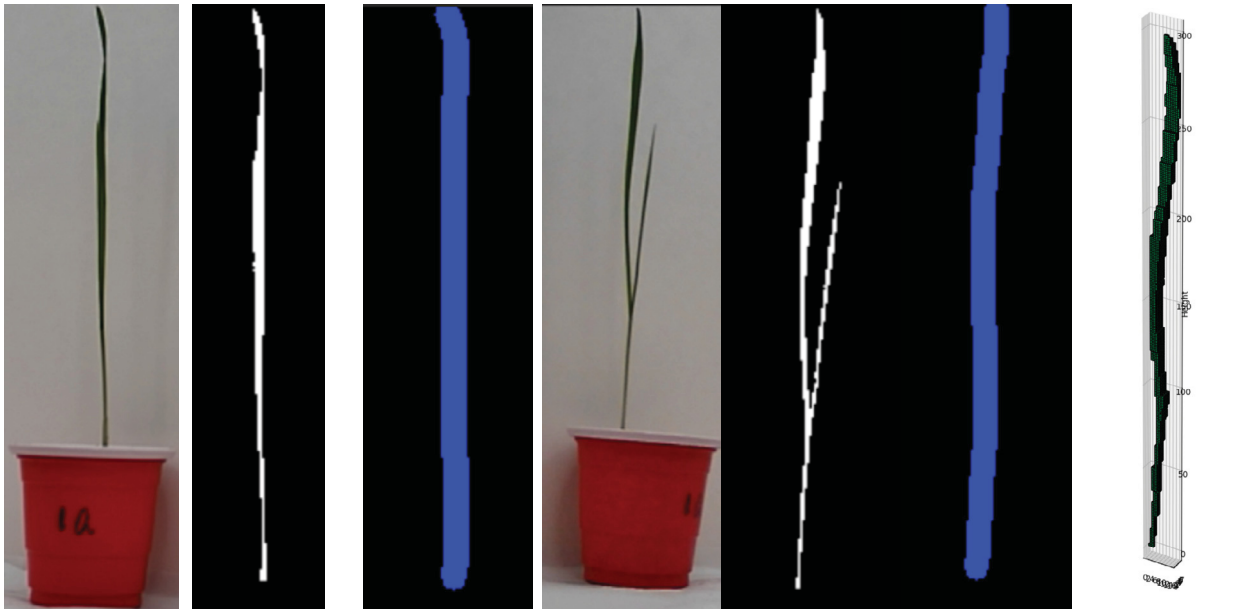

(a) C1 Raw Image (b) C1 Green Mask (c) C1 BFS Path (d) C2 Raw Image (e) C2 Green Mask (f) C2 BFS Path (g) 3D Representation

Fig. 10. Real images, plant information, and length measurements for group A single plant, day 5.

(a) C1 Raw Image (b) C1 Chosen Plant (c) C1 BFS Path (d) C2 Raw Image (e) C2 Chosen Plant (f) C2 BFS Path (g) 3D Representation

Fig. 11. Real images, plant information, and length measurements for group B triple plants, day 1.

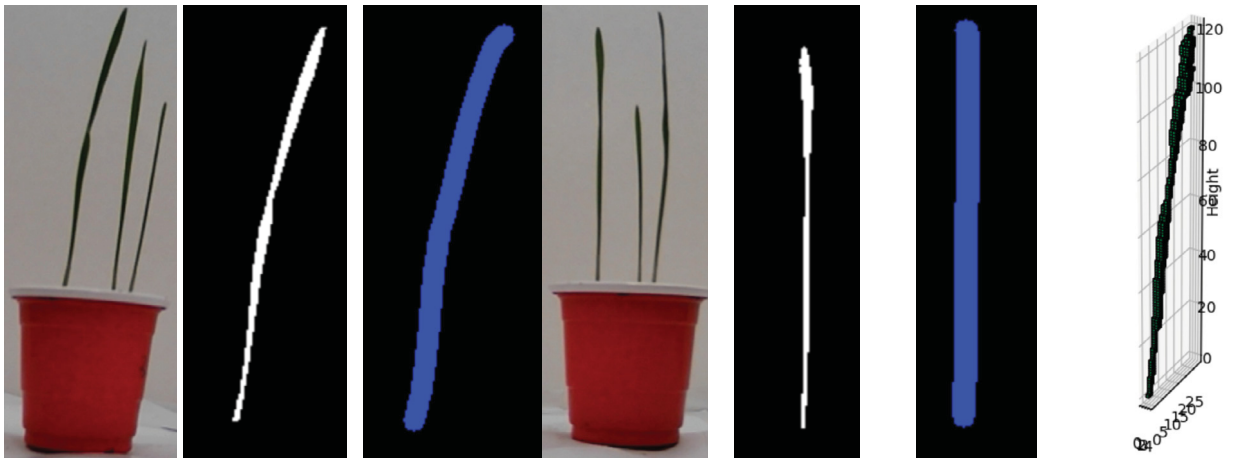

(a) C1 Raw Image (b) C1 Chosen Plant (c) C1 BFS Path (d) C2 Raw Image (e) C2 Chosen Plant (f) C2 BFS Path (g) 3D Representation

Fig. 12. Real images, plant information, and length measurements for group B triple plants, day 3.

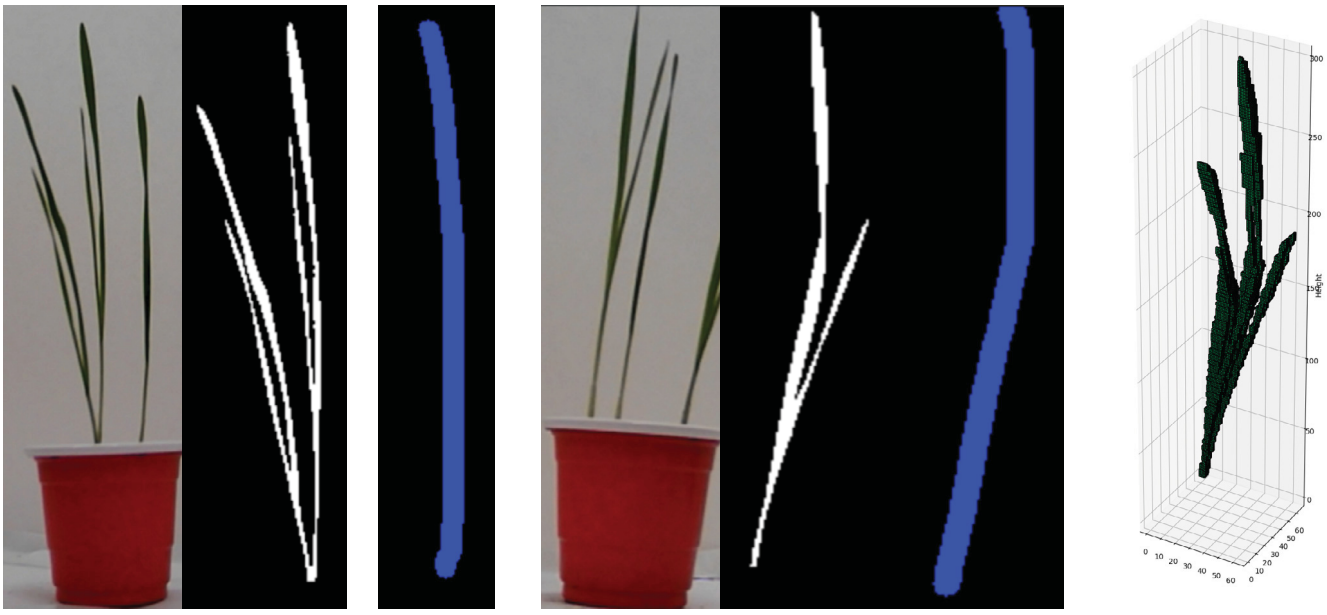

(a) C1 Raw Image (b) C1 Chosen Plant (c) C1 BFS Path (d) C2 Raw Image (e) C2 Chosen Plant (f) C2 BFS Path (g) 3D Representation

Fig. 13. Real images, plant information, and length measurements for group B triple plants, day 5.

Any error present for the 2D algorithm is primarily attributed to the camera angle.

If neither camera captures the entire length of the plant without obstruction or an unideal perspective, then there exists a slight error in the image used for length calculation. Because our setup involves two cameras positioned 90 degrees apart, the maximum misrepresentation of the plant occurs when there's a 45-degree difference between the direction of the plant's curve and each camera's direction, with the plant being parallel to the floor. In such cases, the error due to plant placement is $1 - \frac{1}{\sqrt{2}}$, amounting to approximately 29.3%.

Fig. 15 below is a pictorial representation of such a scenario in a bird's-eye view. The black boxes represent each camera, and the red circle containing the green line represents the potted plant.

To mitigate this error, one might consider the use of additional cameras. For instance, employing three cameras and positioning them on three sides of a hexagonal box would reduce the maximum underestimation to $1 - \frac{\sqrt{3}}{2}$, which is around 13.4%. Further, using simple trigonometry, we can deduce that the maximum percent underestimation for n cameras is $1 - \cos\left(\frac{\pi}{2n}\right)$.

However, our data indicates that the actual percent error observed due to plant placement is significantly lower than these theoretical maximums. This discrepancy is likely attributed to the fact that plants do not typically grow perfectly parallel to the floor.

In addition to the primary error source, there are several minor factors that contribute to measurement inaccuracies. Because the BFS path moves through vertical, horizontal, or diagonal directions, when the plant is tilted at different angles, the program provides different measurements due to pixel discretization, which can be reduced by smoothening the profile through some filters.

The 3D algorithm eliminates the problem of camera angle; however, voxel discretization error may occur. Because voxels are cubes, it is computationally difficult to render the 3d image in its original res-

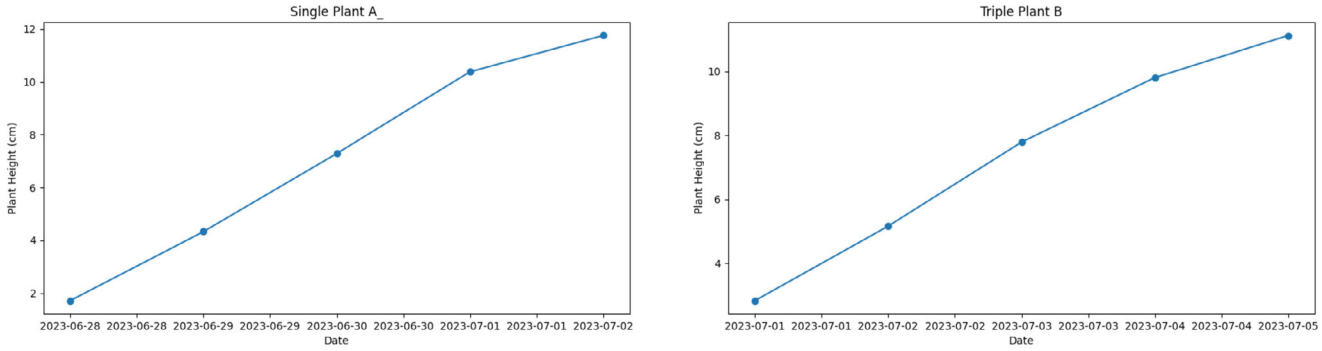

(a) Group A - single plant (2D algorithm)

(b) Group B - triple plants (2D algorithm)

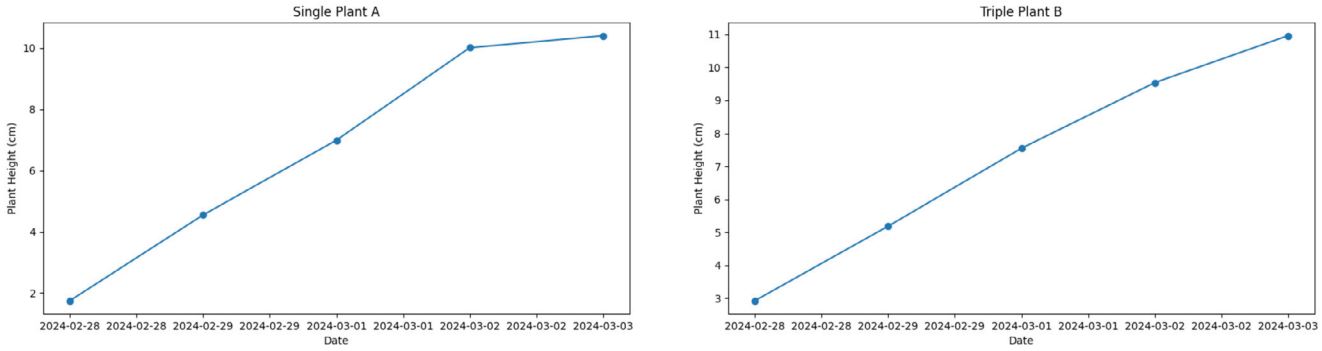

(c) Group A - single plant (3D algorithm)

(d) Group B - triple plants (3D algorithm)

Fig. 14. Length vs. time output tables and charts.

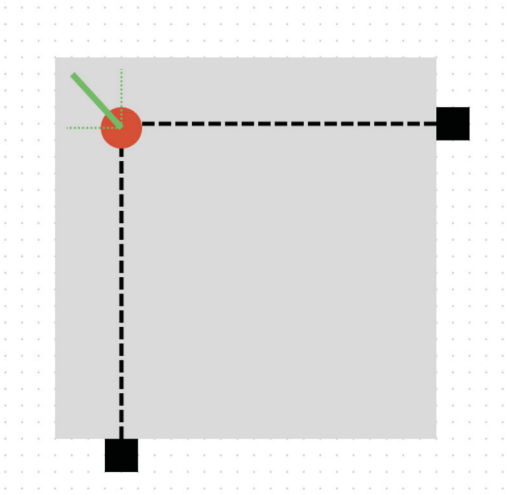

Fig. 15. A bird's-eye view of the worst possible situation.

olution, and a downsampled image must be used. Thus, as the plants grow larger, the algorithm becomes increasingly inaccurate unless the amount of voxels used is increased, although the exact percent error depends on computational power and the amount of voxels used for the calculation.

For days 1 to 4, it was sufficient to render the plants using an arbitrary height of 120 voxels, but as the plant grew larger on days 5, it became apparent that a height of 120 voxels was not enough. If the ratio between the height of the plant and the thickness of the plant is more than the number of voxels used to represent the height, then the algorithm may malfunction as the thickness of the plant is considered less than 1 voxel. Only when the height was increased to 300 voxels was the algorithm able to correctly model the stem.

For human measurements, we found two viable ways to measure the plant, each with its own forms of error. Unlike the computer algorithms, neither of these two methods are automatic.

One method to measure the plant is to bend it straight and find its height against a ruler, but this may stretch or compress the plant and soil, causing inaccuracies. Furthermore, the process of straightening the plant may damage it, negatively affecting plant health and hindering growth.

Another method is to use a bendable object, such as a pipe cleaner, to mold the approximate shape of the plant next to it so that the real plant remains undisturbed. However, this requires extensive human estimation, which may cause significant inaccuracies to arise.

The method used to gather the data for the "Human Measurement" row in Table 1 was the first, albeit with excessive care, so as not to disturb the growth of the plant. This additional caution placed on avoiding plant disturbance may have caused significant inaccuracies in the reported heights, although the exact extent is unquantifiable.

5. Future work for greenhouse plant growth monitoring

As the work is an early-stage study of automatic plant growth monitoring, future work will be implemented to bring it to practical application. Monitoring single or several plants is important for building the model, but the model needs to be tailored for specific plants with different shapes or grow patterns, particularly when large-scale plant farms are under inspection. Besides wheatgrass, different food plants may have different growth behavior and may need different modeling methods. The growth rate in length as critical raw data, may not fully reflect the plant growth health, which also includes flowering, graining/fruiting, diseases, pest impact, etc. Moreover, correlating the growth rate with irrigation, weeding control, temperature, humidity, light, and nutrients should provide a bigger picture of how to optimize the growth conditions, save resources and effort, and eventually enhance crop yielding.

With the imaging method and software validated, we will implement this program in ongoing smart greenhouse development and construction for plant growth monitoring as follows:

1. Given a plant with a typical growth curve and life cycle, we will sample the plants for growth monitoring and select appropriate camera resolution and focus distance;
2. Calibrate the camera noise and determine the image-taken intervals for plant growth monitoring;
3. Daily analysis of the plant growth rate is conducted in comparison with the reference growth curve, which may trigger additional intervention when an abnormal growth pattern is identified;
4. Report the plant growth curve integrated with the environmental control settings, and energy, water, fertilizer consumption.

The plant growth monitoring system will be a critical part in future smart greenhouses. The program can also be extended from length to area or volumetric growth of the plants with higher resolution to optimize the real-time environmental control for maximized plant yielding and carbon neutralization. This software can not only automate future greenhouse operations by communicating with the greenhouse environmental sensing and control system but also provide physics-based data for machine learning to create better plant growth recipes with lower costs in energy, water, and fertilizer supplies.

Besides ground-based fixed cameras in greenhouses, remote cameras onboard, such as satellites or drones, can provide an even larger scale of monitoring the farm plant growth by the leaves area instead and generate even “bigger” data for artificial intelligence and machine learning to create more meaningful guidance to predict greenhouse performance, identify potential problems, optimize planting management, and maximize the plant yielding. Some limitations and challenges are anticipated in the growth monitoring: 1) Different plants exhibit different geometries and shapes, and the plant growth may be evaluated by area or volume better than length, and the algorithm can be extended in the future. 2) The performance of the hardware changes under different environmental conditions, and system reliability may be weak under extreme weather conditions. Higher redundancy of the working capacity of the hardware is recommended. 3) When the technology is scaled up for large-scale operations, multiple cameras will be needed, and the coverage of each camera shall be carefully tuned to avoid blind spots or large overlaps.

6. Conclusions

The camera-based automatic plant growth monitoring system was designed, developed, and demonstrated in monitoring and detecting wheatgrass growth progress for one and three units without human interference. The experiments show the high fidelity and high efficiency of the algorithm. Image processing and plant information extraction was conducted by a Python program, and two novel algorithms for 2D and 3D length estimation were developed to measure the plant length regardless of the growing direction. The program generated dataset and output tables for greenhouse plant growth monitoring. The low-cost camera system is robust for complicated plant growth conditions, displaying higher degrees of accuracy and less plant interference than human measurement. This program can be further refined by reducing pixel and voxel discretization to further smoothen curves or by increasing the number of cameras to obtain more angles of the plant for the algorithms to utilize. This camera-based automatic plant growth monitoring program will be implemented in future smart greenhouse operations.

CRediT authorship contribution statement

Tony Chen: Validation, Visualization, Data curation, Methodology, Software, Writing – original draft. **Huiming Yin:** Conceptualization, Resources, Supervision, Writing – review & editing.

Declaration of competing interest

The authors declare that they have no known competing financial interests or personal relationships that could have appeared to influence the work reported in this paper.

Data availability

The data that support the findings of this study are available from the corresponding author upon reasonable request.

Acknowledgement

This work is inspired by the ongoing BIPVT greenhouse design and construction sponsored by U.S. Department of Agriculture NIFA #2021-67021-34201 and NIFA SBIR #20233353039686, whose support is gratefully acknowledged. We thank Dr. Mehdi Zadshir for his very constructive review and editing comments of this work.

Appendix A. Supplementary material

Supplementary material related to this article can be found online at https://doi.org/10.1016/j.atech.2024.100449.

References

[1] Andrea Thompson, Here are the stunning heat records set so far this summer, Sci. Am. (July 23, 2023). (Accessed 9 September 2023), https://www.scientificamerican.com/article/here-are-the-stunning-heat-records-set-so-far-this-summer1/.
[2] Renee E. Walker, Christopher R. Keane, Jessica G. Burke, Disparities and access to healthy food in the United States: a review of food deserts literature, Health Place 16 (5) (2010) 876–884.
[3] Food and agriculture organization of the United Nations, https://www.fao.org/home/en, 2023. (Accessed 9 September 2023).
[4] Kristalina Georgieva, Global food crisis demands support for people, open trade, bigger local harvests, IMF Blog (September 30, 2022), (September 9, 2023) https://www.imf.org/en/Blogs/Articles/2022/09/30/global-food-crisis-demands-support-for-people-open-trade-bigger-local-harvests.
[5] Abigail Rae Cohen, Gerry Chen, Eli Matthew Berger, Sushmita Warrier, Guanghui Lan, Emily Grubert, Frank Dellaert, Yongsheng Chen, Dynamically controlled environment agriculture: integrating machine learning and mechanistic and physiological models for sustainable food cultivation, ACS ES&T Eng. 2 (1) (2021) 3–19.
[6] Giovanni Avola, Alessandro Matese, Ezio Riggi, An Overview of the Special Issue on “Precision Agriculture Using Hyperspectral Images”, Remote Sens. 15 (7) (2023) 1917.
[7] Huiming Yin, Mehdi Zadshir, Frank Pao, Building Integrated Photovoltaic Thermal Systems: Fundamentals, Designs and Applications, Academic Press, 2021.
[8] Tri Wahyu Saputra, Rudiati Evi Masithoh, Balza Achmad, Development of plant growth monitoring system using image processing techniques based on multiple images, in: Proceeding of the 1st International Conference on Tropical Agriculture, Springer, 2017, pp. 647–653.
[9] Yin-Syuen Tong, Tou-Hong Lee, Kin-Sam Yen, Deep learning for image-based plant growth monitoring: a review, Int. J. Eng. Technol. Innov. 12 (3) (2022).
[10] A. Manikandan, S. Senthilkumar, R. Kannan, A review on automatic monitoring of plant growth and health, Int. J. Agric. Biol. Eng. 12 (4) (2019) 1–16.
[11] Cheng Li, Ranjeeta Adhikari, Yuan Yao, Alexander G. Miller, Kirby Kalbaugh, Daoliang Li, Krishna Nemali, Measuring plant growth characteristics using smartphone based image analysis technique in controlled environment agriculture, Comput. Electron. Agric. 168 (2020) 105123.
[12] Risa Shinoda, Ko Motoki, Kensho Hara, Hirokatsu Kataoka, Ryohei Nakano, Tetsuya Nakazaki, Ryozo Noguchi, Rosetracker: a system for automated rose growth monitoring, Smart Agric. Technol. (2023) 100271.
[13] M.A. Al-Karaki, Automatic monitoring of plant growth for precision agriculture, IEEE Trans. Precis. Agric. 18 (2) (2018) 233–245.
[14] Y. Zhang, C. Wang, Y. Zhao, A survey on automatic plant monitoring and diagnosis systems, Sensors 16 (12) (2016) 2660.

[15] Guoqing Hu, Fengqi You, Renewable energy-powered semi-closed greenhouse for sustainable crop production using model predictive control and machine learning for energy management, Renew. Sustain. Energy Rev. 168 (2022) 112790.
[16] Chiara Bersani, Ahmed Ouammi, Roberto Sacile, Enrico Zero, Model predictive control of smart greenhouses as the path towards near zero energy consumption, Energies 13 (14) (2020) 3647.
[17] Huiming Yin, Gan Song, Liangliang Zhang, Chunlin Wu, The Inclusion-Based Boundary Element Method (iBEM), Academic Press, 2022.
[18] Wei-Han Chen, Neil S. Mattson, Fengqi You, Intelligent control and energy optimization in controlled environment agriculture via nonlinear model predictive control of semi-closed greenhouse, Appl. Energy 320 (2022) 119334.
[19] Chiara Bersani, Marco Fossa, Antonella Priarone, Roberto Sacile, Enrico Zero, Model predictive control versus traditional relay control in a high energy efficiency greenhouse, Energies 14 (11) (2021) 3353.
[20] Sanket Mehta, Arpita Patel, Jagrat Mehta, CCD or CMOS image sensor for photography, in: 2015 International Conference on Communications and Signal Processing (ICCSP), April 2015.
[21] M.A. Al-Karaki, M.A. Al-Hammadi, Hyperspectral imaging for precision agriculture: a review, IEEE Trans. Geosci. Remote Sens. 53 (12) (2015) 6566–6584.
[22] C. Savvides, V. Karagiannidis, I.D. Moschos, Infrared thermography applied to tree health assessment: a review, Sensors 22 (1) (2022) 41.
[23] Thomas H. Cormen, Charles E. Leiserson, Ronald L. Rivest, Clifford Stein, Introduction to Algorithms, MIT Press, 2009.